

# Journal Pre-proof

Magnetically separable humic acid-functionalized magnetite for reductive adsorption of tetrachloroaurate(III) ion in aqueous solution

Sri Juari Santosa (Conceptualization) (Resources) (Supervision) (Writing - review and editing) (Project administration) (Funding acquisition), Philip Anggo Krisbiantoro (Formal analysis) (Investigation) (Writing - original draft) (Visualization), Mustika Yuniarti (Formal analysis) (Investigation) (Funding acquisition), Kustomo (Formal analysis) (Investigation), Soerja Koesnarpardi (Formal analysis) (Investigation)



PII: S2215-1532(21)00029-5

DOI: <https://doi.org/10.1016/j.enmm.2021.100454>

Reference: ENMM 100454

To appear in: *Environmental Nanotechnology, Monitoring & Management*

Received Date: 27 September 2020

Revised Date: 20 February 2021

Accepted Date: 3 March 2021

Please cite this article as: Santosa SJ, Krisbiantoro PA, Yuniarti M, Kustomo, Koesnarpardi S, Magnetically separable humic acid-functionalized magnetite for reductive adsorption of tetrachloroaurate(III) ion in aqueous solution, *Environmental Nanotechnology, Monitoring and Management* (2021), doi: <https://doi.org/10.1016/j.enmm.2021.100454>

This is a PDF file of an article that has undergone enhancements after acceptance, such as the addition of a cover page and metadata, and formatting for readability, but it is not yet the definitive version of record. This version will undergo additional copyediting, typesetting and review before it is published in its final form, but we are providing this version to give early visibility of the article. Please note that, during the production process, errors may be discovered which could affect the content, and all legal disclaimers that apply to the journal pertain.

© 2020 Published by Elsevier.

*Submitted for publication in Environmental Nanotechnology, Monitoring and Management*

(Ref. No. ENMM-D-20-00170R1)

**Magnetically separable humic acid-functionalized magnetite for reductive adsorption of tetrachloroaurate(III) ion in aqueous solution**

Sri Juari Santosa<sup>a\*</sup>, Philip Anggo Krisbiantoro<sup>b,c</sup>, Mustika Yuniarti<sup>a</sup>, Kustomo<sup>d</sup>, Soerja Koesnarpardi<sup>e</sup>

<sup>a</sup>Department of Chemistry, Faculty of Mathematics and Natural Sciences, Universitas Gadjah Mada, Bulaksumur, Yogyakarta 55281, Indonesia

<sup>b</sup>International Graduate Program of Molecular Science and Technology (NTU-MST), National Taiwan University, No. 1, Sec. 4, Roosevelt Road, Taipei 10617, Taiwan

<sup>c</sup>Molecular Science and Technology, Taiwan International Graduate Program, Academia Sinica, Taipei, 11529, Taiwan

<sup>d</sup>Department of Chemistry, Faculty of Science and Technology, State Islamic University of Walisongo, Semarang, Central Java 50185, Indonesia

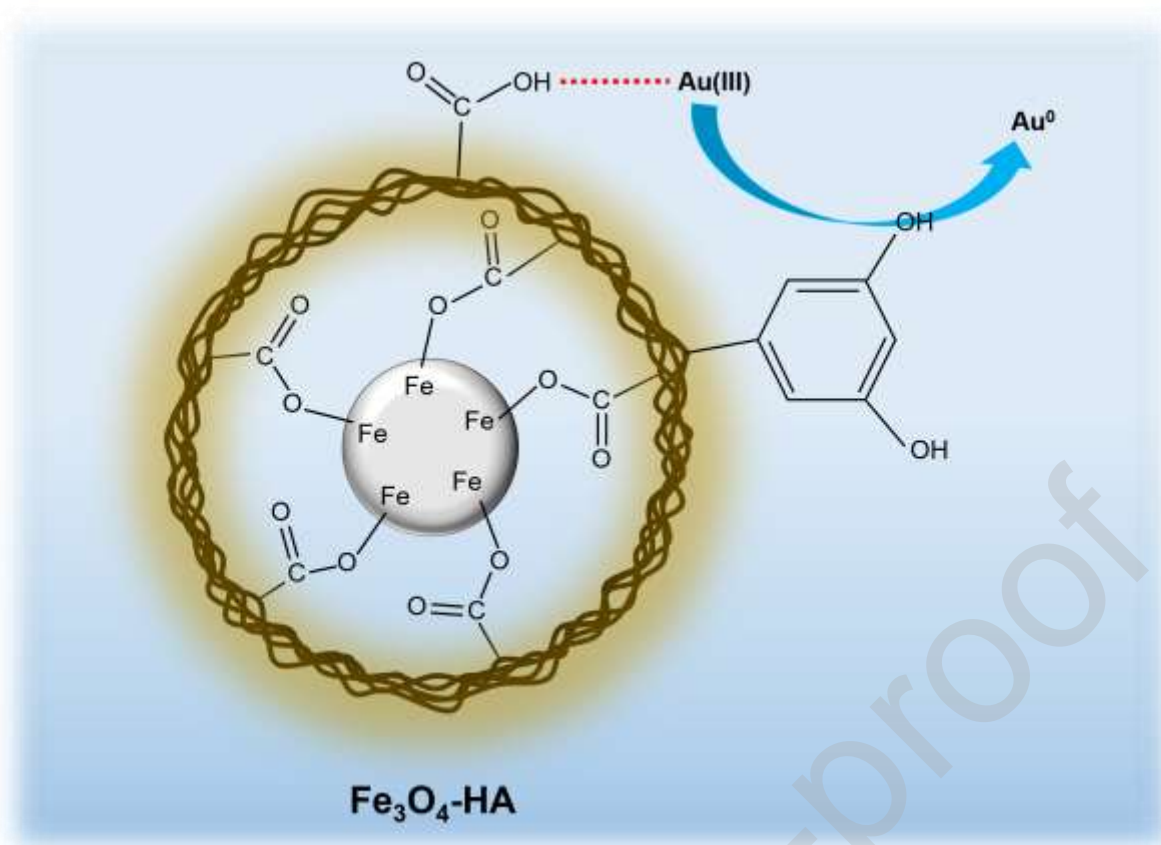
<sup>e</sup>Department of Chemistry, Faculty of Mathematics and Natural Sciences, Universitas Mulawarman, Samarinda 75123, East Kalimantan, Indonesia

\*Corresponding author: [sjuari@ugm.ac.id](mailto:sjuari@ugm.ac.id)

Email: [sjuari@ugm.ac.id](mailto:sjuari@ugm.ac.id)

TEL: +62 81 6426 2984

**Graphical abstract**



### Highlights

- $\text{Fe}_3\text{O}_4\text{-HA}$  was an effective adsorbent for the reductive adsorption of  $\text{Au(III)}$  ion.
- Phenolic  $-\text{OH}$  of HA played a key role on the reduction of  $\text{Au(III)}$  ion into Au.
- The presence of radical scavenger 2-propanol decreased the adsorption of  $\text{Au(III)}$  ion and subsequent reduction to Au.

### Abstract

Recently, it is obvious that the recovery of gold from secondary resources has been of great interest due to its high profitability and vast applications. Among many methods available, reductive adsorption is the easiest, cheapest and eco-friendly way for gold recovery. In the present study, an effective and magnetically separable adsorbent, i.e., humic acid-

functionalized magnetite ( $\text{Fe}_3\text{O}_4\text{-HA}$ ), had been prepared and used for the reductive adsorption of Au(III) ion. The as-prepared  $\text{Fe}_3\text{O}_4\text{-HA}$  was characterized by using a Fourier transform infrared (FTIR) spectrometer, an X-ray diffractometer (XRD), a scanning electron microscopy with an energy dispersive X-ray spectroscopy (SEM-EDS) and a vibrating sample magnetometer (VSM). Quantitative analyses of the total acidity and the content of carboxyl and phenolic  $-\text{OH}$  groups of HA and  $\text{Fe}_3\text{O}_4\text{-HA}$  were also performed. While the experiment results showed that  $\text{Fe}_3\text{O}_4\text{-HA}$  was optimum in adsorbing Au(III) ion at pH 3.5 with adsorption capacity ( $b$ ) according to Langmuir isotherm model was  $200 \text{ mg g}^{-1}$ , the adsorption process followed pseudo-second order with rate constant ( $k_{2p}$ )  $3.03 \times 10^{-4} \text{ g}/(\text{mg}\cdot\text{min})$ . It was found that the phenolic  $-\text{OH}$  group of HA was the one responsible for the reduction of Au(III) ion into metallic gold on the surface of the adsorbent, while the carboxyl group was the active site for the adsorption of Au(III) ion. It was revealed that the presence of radical scavenger 2-propanol decreased the adsorption of Au(III) ion and subsequent reduction to Au. Meanwhile, the adsorbent was easily separated from the medium by an application of an external magnetic field.

**Keywords:** Reductive adsorption, magnetite, humic acid, gold recovery.

## 1. Introduction

The hoarding of electronic waste, so-called e-waste, has been a great burden in many countries for the last two decades. Particularly in developing countries, rapid development of technologies, short-term uses of electronic devices, improper management and inadequate recycling technique have been the major causes for the problems. It was reported that roughly about 40 million metric tons, which is 5% of total solid wastes worldwide, are produced every year (Islam et al., 2020). Not only causing ecological problems, the leaching of heavy metals and other toxic substances have been reported to cause also severe issues for human health

(Chan et al., 2007; Huo et al., 2007; Zhao et al., 2008). To overcome this emerging problem, recycling has become increasingly important.

Since printed circuit board (PCB) is a major component of electronic devices, thus it is one of the major wastes besides plastics, ceramics and glass materials found in e-waste (Zhou and Qiu, 2010). In PCBs from computers and phones, there are many recoverable metals, e.g., copper (Cu), nickel (Ni), iron (Fe), lead (Pb), gold (Au) and palladium (Pd). Among these metals, gold is the most valuable one with an intrinsic value of 67% of all metal components in PCBs (Tuncuk et al., 2012). There are several methods available for gold recovery, including cyanidation, pyrometallurgy, hydrometallurgy, biohydrometallurgy, electrochemistry, amalgamation and leaching with thiosulphate and thiourea (Zhao et al., 2008). However, these techniques are uneconomical, hardly-handled and non-eco. Notably for cyanidation process, the cyanide ion used for gold recovery is highly toxic (Wright, 1964) that if it leaches to the environment, its toxicity is far more lethal than that caused by any other substances in PCBs.

Recently, reductive adsorption has been widely regarded as a promising green technique for gold recovery from secondary resources. Since the first report by Parajuli et al. (Parajuli et al., 2005) that crosslinked lignophenol was able to reduce gold ion into metallic gold, several adsorbents for the process have been reported, including alginic acid (Gao et al., 2017), gallic acid (Santosa et al., 2020a), glutamic acid (Mihăilescu et al., 2019), humic substances (Krisbiantoro et al., 2017; Santosa et al., 2011; Sudiono et al., 2017), salicylic acid (Santosa et al., 2020a) and tannin acid (Liu et al., 2019). Among them, humic acid (HA) as a fraction of humic substances has been reported to be highly potential for reductive adsorption of gold ion owing to the high adsorption capacity and strong reduction potential (Struyk and Sposito, 2001). In terms of the use of HA for the adsorption of gold ion, Lestari (Lestari, 2017) reported that HA isolated from peat soil of South Kalimantan, Indonesia, possessed an adsorption capacity of  $90.91 \text{ mg g}^{-1}$  for Au(III) ion at pH 2 and under room temperature.

Recently, we investigated the role of carboxyl ( $-\text{COOH}$ ) and hydroxyl ( $-\text{OH}$ ) groups of HA in removing Au(III) ion from aqueous solution (Sudiono et al., 2017). It was revealed that the carboxyl group of HA played a key role as the adsorption site for Au(III) ion, while the hydroxyl group was responsible for the reduction of Au(III) ion into metallic gold. Although HA is an excellent adsorbent for gold recovery, it is hardly separated from aqueous solution and thus impractical for real application.

Magnetite ( $\text{Fe}_3\text{O}_4$  or  $\text{Fe}^{2+}\text{Fe}^{3+}_2\text{O}_4$ ) is an iron oxide compound that is a member of the inverse spinel mineral group with isometric space group  $Fd3m$  (Fleet, 1981). The intrinsic magnetic properties of magnetite allow the material to be used for wide ranges of applications, such as storage media, tracking, sensors and separation (Xu et al., 2007); making magnetite is one of the most studied and used minerals in modern era. In terms of adsorption, magnetite has been mainly used as a supporting material to give magnetic properties of the main adsorbent material so that the adsorbent can be easily separated from an aqueous solution with an external magnet. Although the study on the modification of magnetite with HA and its application as an adsorbent for heavy metals have been widely reported (Liu et al., 2008; Rashid et al., 2018, 2017; Singhal et al., 2017), the application for the reductive adsorption of gold ion has not been reported yet.

In the present study, humic acid-functionalized magnetite ( $\text{Fe}_3\text{O}_4\text{-HA}$ ) was prepared through conventional co-precipitation method and used for reductive adsorption of Au(III) ion. HA in this study was isolated from peat soil of Rawa Pening Lake, Central Java, Indonesia. The total acidity and the content of carboxyl and hydroxyl groups of HA before and after being functionalized on magnetite were quantitatively investigated. To evaluate the performance of  $\text{Fe}_3\text{O}_4\text{-HA}$  in adsorbing Au(III) ion, the adsorption parameters including adsorption kinetics and isotherms were investigated. Further, to elucidate the reduction pathway of Au(III) ion on the adsorbent, the effect of electron-scavenging agent, i.e., 2 propanol, was also examined. The

data presented here were partly from the work of a student in our research group, i.e., Mustika Yuniarti, for her undergraduate thesis (Yuniarti, 2013).

## **2. Experimental**

### **2.1 Materials**

Analytical grade  $\text{FeCl}_3 \cdot 6\text{H}_2\text{O}$ ,  $\text{FeSO}_4 \cdot 7\text{H}_2\text{O}$ ,  $\text{HAuCl}_4$ ,  $\text{Ca}(\text{CH}_3\text{COO})_2$ ,  $\text{NH}_3 \cdot \text{H}_2\text{O}$  (25%),  $\text{Ba}(\text{OH})_2$ ,  $\text{HCl}$  (37%) and  $\text{HF}$  were purchased from Merck Co. Inc. (Germany) and used without further purification. Peat soil was obtained from Rawa Pening Lake, Central Java, Indonesia. Meanwhile,  $\text{N}_2$  gas with purity of 99.99% was supplied from CV Perkasa (Indonesia).

### **2.2 Instrumentation**

The apparatuses used in this study were including hot plate equipped with magnetic stirrer (Nouva), analytical balance (Shimadzu), electric pH-meter (Hanna Instrument 211), oven (Fischer Scientific model 655F), centrifuge (Kokusan type H-107), shaker (OSK EFM-60) and siever 200 mesh. For the characterization of the materials, analytical instrumentals, including infra-red spectrometer (Shimadzu FTIR-8201 PC), X-ray diffractometer (Shimadzu XRD-6000), scanning electron microscopy (JEOL JED-2300) and vibrating sample magnetometer (type OXFORD VSM 1.2 H) were used. Meanwhile, the concentration of Au(III) ion was analyzed by using atomic absorption spectroscopy (Analytik Jena).

### **2.3 Isolation of HA**

The isolation of HA was done according to a procedure recommended by the International Humic Substances Society (IHSS). Firstly, peat soil was dried at room temperature and separated from roots and branches. The soil was grinded and sieved to pass through a 200-mesh sieving apparatus. The powder (100 g) was added into 1 L of  $\text{NaOH}$  (0.1

mol L<sup>-1</sup>) and stirred under N<sub>2</sub> atmosphere for 24 h. The supernatant was then separated from the solid by centrifugation at 2000 rpm for 20 min. The supernatant was added by HCl (0.1 mol L<sup>-1</sup>) until pH ≈ 1 and followed by centrifugation at 2000 rpm for 20 min. The precipitate was then dried in an oven at 50 °C overnight to obtain crude HA.

The crude HA was washed by immersing into a mixture solution of HCl (0.1 mol L<sup>-1</sup>) and HF (0.3 mol L<sup>-1</sup>) with a volume ratio of 1:1 in a plastic container. The mixture was stirred for 24 h and aged overnight. The solid of HA was then separated from the solution by centrifugation at 2000 rpm for 20 min. The separated HA was washed by using pure water and finally was dried in an oven at 50 °C overnight.

#### **2.4 Preparation of Fe<sub>3</sub>O<sub>4</sub>-HA**

Fe<sub>3</sub>O<sub>4</sub>-HA was prepared through co-precipitation method by using NH<sub>3</sub>·H<sub>2</sub>O (25%, v/v) as a precipitating agent. Typically, 2.78 g of FeSO<sub>4</sub>·7H<sub>2</sub>O (0.01 mol) and 5.41 g of FeCl<sub>3</sub>·6H<sub>2</sub>O (0.02 mol) were dissolved into 100 mL pure water. The mixture was stirred at 90 °C under N<sub>2</sub> atmosphere. During stirring, 10 mL of NH<sub>3</sub>·H<sub>2</sub>O (25%, v/v) and 1 g of HA were rapidly added. The vigorous stirring was stopped after 30 min and the mixture was then allowed to stand at room temperature. The suspension was separated from filtrate by using a 0.45 μm membrane paper with the help of an external magnet and the obtained solid was washed with pure water to neutral pH. Meanwhile, bare Fe<sub>3</sub>O<sub>4</sub> was prepared in the same manner, except without the addition of HA.

#### **2.5 Stability of Fe<sub>3</sub>O<sub>4</sub> on Fe<sub>3</sub>O<sub>4</sub>-HA**

Fe<sub>3</sub>O<sub>4</sub>-HA (10 mg) was poured into 10 mL of pure water at various pH ranges from 2 to 12 by the addition of HCl (0.1 mol L<sup>-1</sup>) or NaOH (0.1 mol L<sup>-1</sup>) solution. The mixture was then shaken for 120 min and the filtrate was separated from solid by filtering using a 0.45 μm

membrane paper with the help of an external magnet and then was analyzed its Fe content by using atomic absorption spectroscopy.

## 2.6 Determination of total acidity and carboxyl/hydroxyl content

### 2.6.1 Total acidity

Into 20 mL of Ba(OH)<sub>2</sub> (0.1 mol L<sup>-1</sup>) solution, HA (100 mg) or Fe<sub>3</sub>O<sub>4</sub>-HA (100 mg) was poured under N<sub>2</sub> atmosphere. The mixture was shaken for 24 h and the suspension was filtered by using a 0.45 μm membrane paper while retaining Fe<sub>3</sub>O<sub>4</sub>-HA inside the reacting flask using an external magnet. The solid was then rinsed with 20 mL of CO<sub>2</sub>-free pure water. It should be noted that CO<sub>2</sub>-free pure water was obtained by slowly bubbling pure water with N<sub>2</sub> gas for 30 min just before its utilization. The rinse water was mixed with the filtrate and was titrated by HCl (0.05 mol L<sup>-1</sup>) until pH 8.4. As a control, a blank solution in the absence of HA and Fe<sub>3</sub>O<sub>4</sub>-HA was also treated in the same manner as solutions with samples. The total acidities of HA and Fe<sub>3</sub>O<sub>4</sub>-HA were then calculated by the following equation:

$$\text{Total acidity (cmol kg}^{-1}\text{)} = \frac{(V_b - V_s) \times M \times 10^5}{W_s} \quad (1)$$

where M, V<sub>b</sub>, V<sub>s</sub> and W<sub>s</sub> are the molarity of standard HCl solution, volume of standard HCl used for the titration of blank solution, volume of standard HCl solution used for the titration of sample solution and weight of sample, respectively.

### 2.6.2 Carboxyl content

HA (100 mg) or Fe<sub>3</sub>O<sub>4</sub>-HA (100 mg) was poured into an Erlenmeyer flask and was subsequently added with 10 mL of Ca(CH<sub>3</sub>COO)<sub>2</sub> solution (0.5 mol L<sup>-1</sup>) and 40 mL CO<sub>2</sub>-free pure water under N<sub>2</sub> atmosphere. The mixture was shaken for 24 h and the suspension was

filtered by using a 0.45  $\mu\text{m}$  membrane paper with the help of an external magnet. The solid was rinsed with 10 mL  $\text{CO}_2$ -free pure water. Further, the rinse water was mixed with the filtrate and was titrated by NaOH ( $0.1 \text{ mol L}^{-1}$ ) until pH 9.8. The content of carboxyl group of HA and  $\text{Fe}_3\text{O}_4$ -HA was calculated according to the following equation:

$$\text{Carboxyl content (cmol kg}^{-1}\text{)} = \frac{(V_s - V_b) \times M \times 10^5}{W_s} \quad (2)$$

where M is the molarity of standard NaOH solution,  $V_b$  is the volume of standard NaOH used for the titration of blank solution,  $V_s$  is the volume of standard NaOH solution used for the titration of sample solution and  $W_s$  is weight of sample, respectively.

### 2.6.3 Phenolic hydroxyl content

The phenolic  $-\text{OH}$  content was calculated by simply subtracting the total acidity with carboxyl content (Eq. (3)).

$$\text{Phenolic } -\text{OH content (cmol kg}^{-1}\text{)} = \text{Total acidity} - \text{carboxyl content} \quad (3)$$

## 2.7 Reductive adsorption of Au(III) ion

### 2.7.1 Effect of pH

A series of 10 mL of Au(III) ion ( $50 \text{ mg L}^{-1}$ ) solutions was prepared and their acidity was adjusted to pH ranging from 2 to 10. Into the solutions,  $\text{Fe}_3\text{O}_4$ -HA (10 mg) was poured and the mixture was shaken for 15 h. The filtrate was separated from adsorbent by pouring-out the solution through a 0.45  $\mu\text{m}$  membrane paper with the help of an external magnet. The filtrate was then analyzed by using atomic absorption spectroscopy.

### 2.7.2 Adsorption kinetics

Fe<sub>3</sub>O<sub>4</sub>-HA (10 mg) was firstly poured into a series of 10 mL of Au(III) ion (50 mg L<sup>-1</sup>) solutions at optimum pH and every mixture was shaken at different contact times ranging from 5 to 1500 min. Subsequently, the filtrate was separated by pouring-out the solution through a 0.45 μm membrane paper while retaining Fe<sub>3</sub>O<sub>4</sub>-HA inside the reacting flask using an external magnet. The filtrate was then analyzed by using atomic absorption spectroscopy. To evaluate the adsorption mechanism, three kinetic models were used:

- (i) First order kinetic model by Santosa and Muzakky (Suyanta et al., 2010), which

was evaluated from the plot of  $\frac{\ln(\frac{C_o}{C_a})}{C_a}$  versus  $\frac{t}{C_a}$  (Eq. (4)).

$$\frac{\ln(\frac{C_o}{C_a})}{C_a} = k \cdot \frac{t}{C_a} + K \quad (4)$$

- (ii) First order reaching equilibrium was calculated by using Langmuir-Hinshelwood kinetic model (Jin et al., 1996). This model was calculated based on the linearity of

plot of  $\frac{\ln(C_o/C_a)}{C_o-C_a}$  versus  $\frac{t}{C_o-C_a}$  from Eq. (5).

$$\frac{\ln(\frac{C_o}{C_a})}{C_o-C_a} + K = \frac{k_1 p \cdot t}{C_o-C_a} \quad (5)$$

- (iii) Pseudo-second order by using Ho and McKay kinetic model (Ho and McKay, 1999),

which based on the plot of  $\frac{t}{q_t}$  versus  $t$  (Eq. (6)).

$$\frac{t}{q_t} = \frac{1}{k_{2p} q_e^2} + \frac{1}{q_e} t \quad (6)$$

where  $C_0$  and  $C_a$  are the initial and remaining concentration of Au(III) ion ( $\text{mg L}^{-1}$ ) at contact time  $t$ , respectively.  $t$  is the contact time (min), while  $K$  is the equilibrium constant.  $q_e$  and  $q_t$  are the adsorbed amount of Au(III) ion ( $\text{mg g}^{-1}$ ) at equilibrium and contact time  $t$ , respectively.  $k_1$ ,  $k_{1p}$  and  $k_{2p}$  are first order, first order reaching equilibrium and pseudo-second order rate constants, respectively.

### 2.7.3 Adsorption isotherms

$\text{Fe}_3\text{O}_4\text{-HA}$  (10 mg) was added into a series of 10 mL of Au(III) ion solution at various initial concentrations ranging from 0 to 400  $\text{mg L}^{-1}$  and at optimum pH obtained from the experiment of the effect of pH. All mixtures were shaken at equilibrium time obtained from the experiment of adsorption kinetics and followed by immediate separation of filtrates by using a 0.45  $\mu\text{m}$  membrane paper while retaining  $\text{Fe}_3\text{O}_4\text{-HA}$  inside the reacting flask using an external magnet. The filtrate was then analyzed by using atomic absorption spectroscopy. Two isotherm models were used to estimate the adsorption capacity and surface behavior of  $\text{Fe}_3\text{O}_4\text{-HA}$ :

- (i) Langmuir isotherm model, with adsorption capacity ( $b$ ) and equilibrium constant ( $K_L$ ) were estimated from the slope and intercept of plot between  $C/m$  and  $C$  from Eq. (8).

$$m = \frac{b K C}{1 + K C} \quad (\text{Nonlinear}) \quad (7)$$

$$\frac{C}{m} = \frac{1}{b K} + \frac{C}{b} \quad (\text{Linear}) \quad (8)$$

- (ii) Freundlich isotherm model, with the removal capacity of Freundlich model ( $B$ ) was determined from the intercept of plot between  $\log m$  and  $\log C$  (Eq. (10)).

$$m = B C^{1/n} \quad (\text{Nonlinear}) \quad (9)$$

$$\log m = \log B + \frac{1}{n} \log C \quad (\text{Linear}) \quad (10)$$

where  $m$  is the amount of adsorbed Au(III) ion,  $b$  is Langmuir's adsorption capacity corresponding to energetically complete monolayer coverage,  $K$  is the equilibrium constant,  $C$  is the equilibrium concentration of Au(III) ion in solution,  $B$  is the Freundlich's removal capacity and  $n$  is a constant.

### 2.8 Effect of 2-propanol

Fe<sub>3</sub>O<sub>4</sub>-HA (5 mg) was added into 10 mL of Au(III) ion solution at optimum pH and concentration from the previous experiments. Into the mixture, 2-propanol was added with concentrations were varied from 2 to 50% (v/v). The mixture was then shaken at the optimum time obtained from the adsorption kinetics experiment. The filtrate was filtered by using a 0.45 μm membrane paper while retaining Fe<sub>3</sub>O<sub>4</sub>-HA inside the reacting flask using an external magnet. The filtrate was then analyzed for the content of its remaining Au(III) ion by using atomic absorption spectroscopy.

## 3 Results and discussion

### 3.1 Characteristics of HA and Fe<sub>3</sub>O<sub>4</sub>-HA

#### 3.1.1 XRD

Figure 1 shows the XRD spectra of purified HA, Fe<sub>3</sub>O<sub>4</sub> and Fe<sub>3</sub>O<sub>4</sub>-HA. As expected, purified HA showed no diffraction lines (Fig. 1a), which means that the as-extracted HA was

completely free from the inorganic impurities. As shown in Fig. 1b,  $\text{Fe}_3\text{O}_4$  gave six typical diffraction lines at  $2\theta = 30.28, 35.60, 43.30, 53.62, 57.22$  and  $62.82^\circ$  which assignable to (220), (311), (400), (422), (511) and (440) planes, respectively, of cubic structure. Meanwhile,  $\text{Fe}_3\text{O}_4$ -HA gave the same diffraction lines as that of pristine  $\text{Fe}_3\text{O}_4$ , while the intensities of these peaks were all decreased (Fig. 1c). This implies that the modification of  $\text{Fe}_3\text{O}_4$  with HA did not change the geometrical structure of  $\text{Fe}_3\text{O}_4$  but may decrease the crystallinity of  $\text{Fe}_3\text{O}_4$ . In addition, the crystallite sizes estimated by applying Debye-Scherrer to the highest diffraction lines at  $35.60$  and  $35.64$  for pristine  $\text{Fe}_3\text{O}_4$  and modified  $\text{Fe}_3\text{O}_4$ , respectively, were  $19.20$  and  $15.30$  nm.

### 3.1.2 FTIR

FTIR spectra of crude and purified HA,  $\text{Fe}_3\text{O}_4$  and  $\text{Fe}_3\text{O}_4$ -HA are given in Fig. 2. As displayed in Fig. 2a-b, both crude and purified HA possessed common absorption bands at  $3425, 2924$  and  $1627\text{ cm}^{-1}$ , which can be ascribed to O-H stretching from phenolic groups, aliphatic C-H asymmetric stretching and C-O asymmetric stretching in  $-\text{COO}^-$ , respectively. While the appearance of absorption bands at  $1404, 540$  and  $470\text{ cm}^{-1}$  indicate that metal ions impurities exist in crude HA (Fig. 2a), a peak at  $1033\text{ cm}^{-1}$  is highly likely to correspond to siliceous compounds. These peaks were eventually diminished after purification with HF solution (Fig. 2b). This supports the previously mentioned fact that the diffraction line due to inorganic crystal was not found on the XRD spectra of purified HA (Fig. 1a). The purification process also enhanced the absorption bands of the aliphatic C-H asymmetric stretching and leads to the appearance of C=O stretching of carboxyl groups at  $2924$  and  $1705\text{ cm}^{-1}$ , respectively (Fig. 2b).

As given in Fig. 2c,  $\text{Fe}_3\text{O}_4$  displayed three typical absorption bands at  $3425, 1627$  and  $578\text{ cm}^{-1}$ , which assignable to O-H stretching of surface hydroxyl groups, O-H bending and

Fe–O stretching, respectively. After Fe<sub>3</sub>O<sub>4</sub> was modified with HA (Fig. 2d), while the absorption bands at 3425 and 1627 cm<sup>-1</sup> were increased, new peaks were observed at wavenumber 1404 and 1118 cm<sup>-1</sup>. These peaks are due to the stretching vibration of C=O and C–O of free carboxyl groups which interact with FeO of Fe<sub>3</sub>O<sub>4</sub> (Koesnarpadi et al., 2015; Liu et al., 2008; Yantasee et al., 2007). Since the preparation of Fe<sub>3</sub>O<sub>4</sub>-HA was performed under basic condition (pH ≈ 10), the possible reaction between HA and Fe<sub>3</sub>O<sub>4</sub> is a ligand-exchange reaction between –COO<sup>-</sup> and surface hydroxyl groups of Fe<sub>3</sub>O<sub>4</sub> (Eq. (11)) (Koesnarpadi et al., 2015).



### 3.1.3 SEM-EDS

Fig. 3 shows the SEM images and EDS analyses of HA, Fe<sub>3</sub>O<sub>4</sub> and Fe<sub>3</sub>O<sub>4</sub>-HA, while Table 1 summarizes the percentage of the mass of elements on the sample from EDS analysis. HA has an irregular structure and size with smooth surface (Fig. 3a), while Fe<sub>3</sub>O<sub>4</sub> shows smaller in particle size with rougher and brighter surface (Fig. 3b). When HA was functionalized on Fe<sub>3</sub>O<sub>4</sub> to form Fe<sub>3</sub>O<sub>4</sub>-HA, the surface of HA appeared to be modified by rough-bright spots of Fe<sub>3</sub>O<sub>4</sub> (Fig. 3c). Meanwhile, from EDS analysis, the functionalization of HA on Fe<sub>3</sub>O<sub>4</sub> decreased the percentage of C and Fe atoms of pure HA and pristine Fe<sub>3</sub>O<sub>4</sub>, respectively (Table 1). Notably for Fe atom, the significant decrease in the percent mass, i.e., from 54.21 to 24.93%, implies that HA was successfully coated the surface of Fe<sub>3</sub>O<sub>4</sub>. We have previously reported similar results on the SEM images and EDS analyses of HA, Fe<sub>3</sub>O<sub>4</sub> and Fe<sub>3</sub>O<sub>4</sub>-HA (Koesnarpadi et al., 2015).

### 3.1.4 Magnetic characterization

The magnetization curve of  $\text{Fe}_3\text{O}_4$  and  $\text{Fe}_3\text{O}_4\text{-HA}$  was measured at room temperature using VSM and the result is shown in Fig. 4. As clearly depicted, the magnetization of both  $\text{Fe}_3\text{O}_4$  and  $\text{Fe}_3\text{O}_4\text{-HA}$  increases with the increasing of the applied magnetic field until it reaches the saturation point. Both materials were paramagnetic with almost zero coercivity with the specific saturation magnetization ( $M_s$ ) of  $\text{Fe}_3\text{O}_4$  ( $71.3 \text{ emu g}^{-1}$ ) was relatively higher than that of  $\text{Fe}_3\text{O}_4\text{-HA}$  ( $63.3 \text{ emu g}^{-1}$ ). This expected result suggests that the functionalization of non-magnetic HA on  $\text{Fe}_3\text{O}_4$  negatively affects the magnetic properties of  $\text{Fe}_3\text{O}_4$ . Nevertheless, it is clear from the conventional magnetic test that  $\text{Fe}_3\text{O}_4\text{-HA}$  is still strongly attracted to the external magnetic field (Fig. 4).

### 3.1.5 Stability of $\text{Fe}_3\text{O}_4$ on $\text{Fe}_3\text{O}_4\text{-HA}$

As shown in Fig. 5, the stability of  $\text{Fe}_3\text{O}_4$  on  $\text{Fe}_3\text{O}_4\text{-HA}$  towards dissolution is high under all tested initial pH. At pH ranging from 2 to 10, the amounts of leached Fe from adsorbent were less than  $0.1 \text{ mmol g}^{-1}$  (> 99% stability), while at pH 11 and 12, the stability was slightly decreased. The increase in the amount of leached Fe under strong basic condition is presumably due to the dissolution of HA from the surface of  $\text{Fe}_3\text{O}_4$ . It must be noted that HA is highly soluble under basic condition (Stevenson, 1994). This detachment of HA further decreases the resistance of  $\text{Fe}_3\text{O}_4$  against dissolution due to the direct contact with  $\text{OH}^-$  in the working solution. Nevertheless, since the amounts of dissolved Fe at pH 11 ( $0.27 \text{ mmol g}^{-1}$ ) and 12 ( $0.42 \text{ mmol g}^{-1}$ ) were very small, it is plausible to mention that  $\text{Fe}_3\text{O}_4$  on  $\text{Fe}_3\text{O}_4\text{-HA}$  is highly stable towards dissolution.

### 3.1.6 Total acidity and carboxyl/hydroxyl content

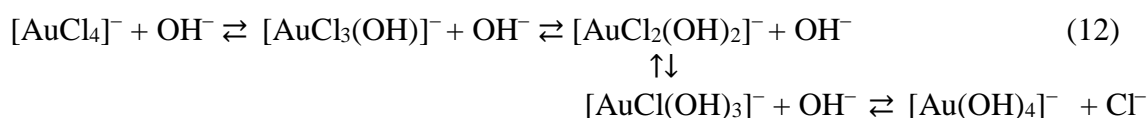
In the present study, the total acidity and the content of carboxyl groups of HA and Fe<sub>3</sub>O<sub>4</sub>-HA were determined through an indirect potentiometric titration by using Ba(OH)<sub>2</sub> (Eq. (1)) and Ca-acetate methods (Eq. (2)) (Stevenson, 1994), respectively. As shown in Table 2, while the total acidity and the content of carboxyl and phenolic –OH groups are within the range of the values reported by Stevenson (Stevenson, 1994), the functionalization of HA on Fe<sub>3</sub>O<sub>4</sub> significantly decreases the total acidity owing mostly to a drastic decrease of carboxyl groups content from 315.79 to 87.43 cmol kg<sup>-1</sup>. This is because, as described in *section 2.4*, the preparation of Fe<sub>3</sub>O<sub>4</sub>-HA was performed under basic condition (pH ≈ 10). At such condition, all carboxyl and mostly phenolic –OH groups are ionized which then readily interact with positively charged Fe<sup>2+</sup> and Fe<sup>3+</sup> on the freshly formed Fe<sub>3</sub>O<sub>4</sub>. The reason for the higher consumption of carboxyl groups, on the other hand, is simply because the ionization degree of carboxyl group is much higher than that of phenolic –OH groups, and thus carboxyl groups are much ready to interact with Fe<sub>3</sub>O<sub>4</sub> than phenolic –OH groups. This supports the previously mentioned fact that the appearance of sharp absorbance at 1404 cm<sup>-1</sup> on Fe<sub>3</sub>O<sub>4</sub>-HA was due to the C=O stretching from carboxylate anion which interacted with Fe–O (Koesnarpadi et al., 2015; Liu et al., 2008; Yantasee et al., 2007).

## 3.2 Adsorption of Au(III) ion

### 3.2.1 Effect of initial pH

As shown in Fig. 6, the adsorption of Au(III) ion is largely affected by the initial pH of the reaction solution. This is because the initial pH is an important parameter that affects the surface charges of the adsorbent as well as the ionic speciation of the adsorbate. Fe<sub>3</sub>O<sub>4</sub>-HA showed high adsorption performance for Au(III) ion under acidic condition (pH 2 - 5), in which pH 3.5 was the optimum condition where complete adsorption of Au(III) ion was achieved

(Fig. 6). At  $\text{pH} > 3.5$ , the adsorption was gradually decreased and even further abruptly decreased after  $\text{pH} 6$ . As we previously found that the adsorption of Au(III) ion on HA isolated from Rawa Pening Lake, Central Java, Indonesia, was solely due to the binding of Au(III) ion (which present as  $\text{AuCl}_4^-$ ) with the protonated carboxyl groups of HA (Sudiono et al., 2017). The effect of  $\text{pH}$  for Au(III) ion on  $\text{Fe}_3\text{O}_4\text{-HA}$  can be explained as follows. Under strong and weakly acidic conditions ( $\text{pH} 2 - 5$ ), the available active carboxyl groups of  $\text{Fe}_3\text{O}_4\text{-HA}$  are highly protonated and hence readily interacts with  $\text{Cl}^-$  from  $\text{AuCl}_4^-$  ion through a hydrogen bonding. As the  $\text{pH}$  increases, the carboxyl groups of HA on  $\text{Fe}_3\text{O}_4\text{-HA}$  deprotonate into carboxyl anions and  $\text{Cl}^-$  on  $\text{AuCl}_4^-$  ion are substituted with  $\text{OH}^-$  to form  $[\text{AuCl}_{4-x}(\text{OH})_x]^-$  complex (Eq. (12)). It must be noted that at  $\text{pH} 5$ , approximately 90% of carboxyl groups are ionized (Muscolo et al., 2013; Santosa et al., 2006). Consequently, the repulsive interaction between carboxyl anions and  $[\text{AuCl}_{4-x}(\text{OH})_x]^-$  complex occurs which then subsequently leads to the decrease in the amount of adsorbed gold ions. This is supported by the fact that the point of zero charge  $\text{pH}$  ( $\text{pH}_{\text{PZC}}$ ) of  $\text{Fe}_3\text{O}_4\text{-HA}$  (calculated by using the  $\text{pH}$ -drift method with the procedure similar to that reported by Nuryono et al., 2020), is 6.47. This means that the adsorbent is negatively charged at  $\text{pH} > 6.47$ . The same behavior was also observed on the adsorption of Au(III) ion on fulvic acid-coated magnetite ( $\text{Fe}_3\text{O}_4\text{-FA}$ ), in which  $\text{pH} 4$  was the optimum condition for the adsorption of Au(III) ion and that carboxyl groups were the responsible active sites for the adsorption process (Krisbiantoro et al., 2017). Such trend was also observed in our previous work on the adsorption of Au(III) ion on HA (Sudiono et al., 2017).



### 3.2.2 Adsorption kinetics

Fig. 7 displays the effect of reaction time on the amounts of adsorbed Au(III) ion on Fe<sub>3</sub>O<sub>4</sub>-HA. The adsorption process was initially rapid at the first 30 min and then gradually increased before reached equilibrium at 900 min. This equilibrium time is indeed much longer than that of immobilized HA (600 min) in our previous report, presumably owing to the much lower carboxyl content (Sudiono et al., 2017).

To evaluate the adsorption behavior of Au(III) ion on Fe<sub>3</sub>O<sub>4</sub>-HA, the effect of time was fitted to first-order (Eq. (4)), first-order reaching equilibrium (Eq. (5)) and pseudo-second order kinetic models (Eq. (6)) by Santosa and Muzakky (Suyanta et al., 2010), Langmuir-Hinshelwood (Jin et al., 1996) and Ho-McKay (Ho and McKay, 1999), respectively. From Table 3, it is obvious that on the basis of correlation coefficient value ( $R^2$ ), the adsorption of Au(III) ion on Fe<sub>3</sub>O<sub>4</sub>-HA followed pseudo-second order kinetic model with  $R^2$  value greater than 0.995. The fact that the  $R^2$  was substantially higher than that of first-order ( $R^2= 0.9869$ ) and first-order reaching equilibrium ( $R^2= 0.9576$ ) implies that the adsorption process inclined towards chemisorption. In this case, the adsorption process is governed by at least two parameters, presumably the number of active sites of adsorbent, i.e., carboxyl groups and the concentration of Au(III) ion.

### 3.2.3 Adsorption isotherms

Since HA is rich in carboxyl and phenolic -OH groups, it is important to investigate the surface behavior and the adsorption capacity of Fe<sub>3</sub>O<sub>4</sub>-HA. In the present study, the adsorption capacity of the adsorbent was evaluated by using Langmuir (Eqs. (7-8)) and Freundlich (Eqs. (9-10)) isotherm models. While Fig. 8 shows the plot of adsorbed Au(III) ion on Fe<sub>3</sub>O<sub>4</sub>-HA versus the remaining concentration of Au(III) ion in the working solution, Table 4 summarizes the parameters obtained from the linear plot of the isotherm models. It is obvious

that the non-linear plots of the experimental data more closely followed the Langmuir isotherm model (Fig. 8). This is supported by the fact that the Langmuir isotherm model gives a better fit than the Freundlich isotherm model on the basis of  $R^2$  value (Table 4). These results simply mean that the coverage of Au(III) ion on Fe<sub>3</sub>O<sub>4</sub>-HA is monolayer owing to the homogeneously distributed active sites of Fe<sub>3</sub>O<sub>4</sub>-HA, presumably by carboxyl groups. The suitability of the Langmuir isotherm model was also observed in our previous report on the adsorption of Au(III) ion on HA and esterified HA (Prasasti et al., 2019) and Fe<sub>3</sub>O<sub>4</sub>-FA (Krisbiantoro et al., 2017). Since the equilibrium parameter values ( $R_L$ ) calculated from an equation of  $R_L = 1/(1 + K_L C_0)$  was between 0 and 1, the adsorption process is favorable. Compared to other adsorbents (Table 5), Fe<sub>3</sub>O<sub>4</sub>-HA exhibited relatively high adsorption capacity towards Au(III) ion, in which it is the second-best of any other adsorbents ever reported just below the esterified HA (Prasasti et al., 2019).

### 3.3 Characterization after adsorption

The XRD and FTIR spectra of Fe<sub>3</sub>O<sub>4</sub>-HA after adsorption of Au(III) ion are shown in Fig. 9 and 10, respectively. After adsorption, Fe<sub>3</sub>O<sub>4</sub>-HA showed new diffraction lines at  $2\theta = 37.97$ ,  $44.16$  and  $64.44^\circ$ , which were assignable to (111), (200) and (220) planes, respectively, of cubic Au. This clearly demonstrated that Fe<sub>3</sub>O<sub>4</sub>-HA was not only effective in adsorbing Au(III) ion but also able to reduce adsorbed Au(III) ion into metallic gold. However, the intensity of diffraction lines due to Fe<sub>3</sub>O<sub>4</sub> was significantly decreased, indicating that the adsorption process leads to a decrease in the crystallinity of the magnetite core. Meanwhile, the addition of a peak with an asterisk may be caused by the formation of goethite ( $\alpha$ -FeOOH) (Salviano et al., 2018).

A stark difference observed on the FTIR spectra of the adsorbent before and after adsorption was the appearance of an absorption band at  $1381\text{ cm}^{-1}$ , which according to Sudiono

et al. (Sudiono et al., 2017) is corresponding to the stretching vibration of carboxyl anion of HA which interacts with gold ions. In addition, the absorption bands due to –OH stretching and bending were decreased. Since it was suggested that phenolic –OH groups of HA are responsible for the reduction of Au(III) ion (Eq. (13)) (Sudiono et al., 2017), it is reasonable to mention that the decrease in the intensity of these absorption bands is due to the oxidation process of phenolic –OH of the adsorbent.



### 3.4 Effect of 2-propanol

Although it has been confirmed that the phenolic –OH group of the adsorbent was the one responsible for the reduction of Au(III) ion, it is still uncertain in which manner the electron is transferred to  $\text{Au}^{3+}$ . Since it was reported that HA is not only a redox-active organic macromolecule but it also contains stable organic free radicals (Steelink and Tollin, 1962), the effect of radical scavenger, that is 2-propanol, was investigated. From XRD spectra, as given in Fig. 9b-d, the addition of 2-propanol significantly decreased the intensities of the diffraction lines of Au. Because the intensity of a diffraction line in XRD spectra is proportional to the population of crystal planes, it is plausible to assume that the addition of 2-propanol is indeed decreasing the amount of reduced Au(III) ion on the surface of adsorbent. Thus, it is most likely that the reduction process of Au(III) ion follows a radical pathway. Meanwhile, through FTIR spectra, the increase of the concentration of 2-propanol added to the reaction solution increased the intensity of –OH stretching ( $3425 \text{ cm}^{-1}$ ). This demonstrated that less phenolic –OH groups were used for the reduction process of Au(III) ion in the presence of 2-propanol.

On the other hand, as shown in Fig. 11, the increasing concentration of the added 2-propanol solution also decreased the removal ability of the adsorbent. In the absence of 2-

propanol, 58% of Au(III) ion was removed and the value was maintained with the addition of 5% (v/v) of 2-propanol. With the addition of 10 and 20% (v/v) of 2-propanol, the percentage of the removed Au(III) ion from the reaction solution slightly decreased to 56 and 51%, respectively. Indeed, these values are rather insignificant. However, the decrease in the amount of removed Au(III) ion became significant when the concentration of 2-propanol is 50%. In such a high concentration of 2-propanol, only 27% of Au(III) ion was removed from the reaction solution. This can be explained as follows. If it is assumed that the reductive adsorption of Au(III) ion on the surface of Fe<sub>3</sub>O<sub>4</sub>-HA is a continuous process where once a carboxyl group of the adsorbent is adsorbing Au(III) ion, phenolic –OH groups are then subsequently reducing Au(III) ion to Au; resulting in a complete detachment of the adsorbed species from the carboxyl group. Consequently, that carboxyl group can do another uptake for Au(III) ion. This process is a continuous reaction until all phenolic –OH groups are oxidized to quinone. At this stage, the equilibrium state is reached. When 2-propanol is added into the reaction solution, electrons from phenolic –OH groups are scavenged and thus they cannot reduce Au(III) ion. As the result, the removal process stopped since the carboxyl group cannot uptake another Au(III) ion. With the increase of the concentration of 2-propanol, more electrons are scavenged and hence the adsorption equilibrium will be reached faster. This is why at high concentration of 2-propanol, i.e., 50% (v/v), the percentage of the removed Au(III) ion is very low (27%  $\approx$  35.5 mg g<sup>-1</sup>).

#### **4 Conclusions**

In the present study, Fe<sub>3</sub>O<sub>4</sub>-HA was synthesized through co-precipitation method and used for the reductive adsorption of Au(III) ion in aqueous solution. While it is apparent that Fe<sub>3</sub>O<sub>4</sub>-HA possessed excellent performance for the reductive adsorption of Au(III) ion, it is magnetically separable, and thus ready to be re-collected from reaction solution. The

adsorption of Au(III) ion on Fe<sub>3</sub>O<sub>4</sub>-HA was optimum at weakly acidic condition, i.e., pH 3.5, with adsorption capacity (*b*) according to Langmuir isotherm model was 200 mg g<sup>-1</sup>. The adsorption process followed pseudo-second order with rate constant (*k<sub>2p</sub>*) 3.03 × 10<sup>-4</sup> g/(mg.min). Phenolic –OH group of HA was the one responsible for the reduction of Au(III) ion into metallic gold on the surface of adsorbent, while carboxyl group was the active site for the adsorption of Au(III) ion. It was revealed that the addition of radical scavenger 2-propanol into the reaction solution decreased the adsorption of Au(III) ion as well as the reduction of Au.

#### **CRedit authorship contribution statement**

- **Sri Juari Santosa:** Conceptualization, Resources, Supervision, Writing – review & editing, Project administration, Funding acquisition.
- **Philip Anggo Krisbiantoro:** Formal analysis, Investigation, Writing – original draft, Visualization.
- **Mustika Yuniarti:** Formal analysis, Investigation, Funding acquisition.
- **Kustomo:** Formal analysis, Investigation.
- **Soerja Koesnarpadi:** Formal analysis, Investigation.

#### **Conflict of interest**

There is no conflict of interest to declare.

#### **Acknowledgements**

The completion of this research was financially supported by the Directorate General of Higher Education, Republic of Indonesia through a research scheme of World Class Research with contract number 892/UN1/DITLIT/DIT-LIT/PT/2020.

## References

- Chan, J.K.Y., Xing, G.H., Xu, Y., Liang, Y., Chen, L.X., Wu, S.C., Wong, C.K.C., Leung, C.K.M., Wong, M.H., 2007. Body loadings and health risk assessment of polychlorinated dibenzo-*p*-dioxins and dibenzofurans at an intensive electronic waste recycling site in China. *Environ. Sci. Technol.* 41, 7668–7674. <https://doi.org/10.1021/es071492j>
- Stevenson, F.J., 1994. *Humus chemistry: Genesis, composition, reactions*, 2nd Edition. John Wiley and Sons. Inc., New York.
- Fleet, M.E., 1981. The structure of magnetite. *Acta Crystall. B-Stru.* 37, 917–920. <https://doi.org/10.1107/S0567740881004597>
- Fujiwara, K., Ramesh, A., Maki, T., Hasegawa, H., Ueda, K., 2007. Adsorption of platinum (IV), palladium (II) and gold (III) from aqueous solutions onto l-lysine modified crosslinked chitosan resin. *J. Hazard. Mater.* 146, 39–50. <https://doi.org/10.1016/j.jhazmat.2006.11.049>
- Gao, X., Zhang, Y., Zhao, Y., 2017. Biosorption and reduction of Au(III) to gold nanoparticles by thiourea modified alginate. *Carbohydr. Polym.* 159, 108–115. <https://doi.org/10.1016/j.carbpol.2016.11.095>
- Ho, Y.S., McKay, G., 1999. Pseudo-second order model for sorption processes. *Process Biochem.* 34, 451–465. [https://doi.org/10.1016/S0032-9592\(98\)00112-5](https://doi.org/10.1016/S0032-9592(98)00112-5)

- Huo, X., Peng, L., Xu, X., Zheng, L., Qiu, B., Qi, Z., Zhang, B., Han, D., Piao, Z., 2007. Elevated blood lead levels of children in Guiyu, an electronic waste recycling town in China. *Environ. Health Perspect.* 115, 1113–1117. <https://doi.org/10.1289/ehp.9697>
- Islam, A., Ahmed, T., Awual, Md.R., Rahman, A., Sultana, M., Aziz, A.A., Monir, M.U., Teo, S.H., Hasan, M., 2020. Advances in sustainable approaches to recover metals from e-waste-A review. *J. Clean. Prod.* 244, 118815. <https://doi.org/10.1016/j.jclepro.2019.118815>
- Jin, X., Bailey, G.W., Yu, Y.S., Lynch, A.T., 1996. Kinetics of single and multiple metal ion sorption processes on humic substances. *Soil Sci.* 161, 509–520. <https://doi.org/10.1097/00010694-199608000-00006>
- Koesnarpadi, S., Santosa, S.J., Siswanta, D., Rusdianto, B., 2015. Synthesis and characterization of magnetite nanoparticle coated humic acid (Fe<sub>3</sub>O<sub>4</sub>/HA). *Procedia Environ. Sci.* 30, 103–108. <https://doi.org/10.1016/j.proenv.2015.10.018>
- Krisbiantoro, P.A., Santosa, S.J., Kunarti, E.S., 2017. Synthesis of fulvic acid-coated magnetite (Fe<sub>3</sub>O<sub>4</sub>-FA) and its application for the reductive adsorption of AuCl<sub>4</sub><sup>-</sup>. *Indones. J. Chem.* 17, 453–460. <https://doi.org/10.22146/ijc.24828>
- Lestari, P., 2017. Isolation of humic acid from peat soil and its application as an adsorbent for AuCl<sub>4</sub><sup>-</sup> in solution. *AIP Conference Proceedings* 1823, 020039. <https://doi.org/10.1063/1.4978112>
- Liu, F., Peng, G., Li, T., Yu, G., Deng, S., 2019. Au(III) adsorption and reduction to gold particles on cost-effective tannin acid immobilized dialdehyde corn starch. *Chem. Eng. J.* 370, 228–236. <https://doi.org/10.1016/j.cej.2019.03.208>

- Liu, J., Zhao, Z., Jiang, G., 2008. Coating Fe<sub>3</sub>O<sub>4</sub> magnetic nanoparticles with humic acid for high efficient removal of heavy metals in water. *Environ. Sci. Technol.* 42, 6949–6954. <https://doi.org/10.1021/es800924c>
- Mihăilescu, M., Negrea, A., Ciopec, M., Davidescu, C.M., Negrea, P., Duțeanu, N., Rusu, G., 2019. Gold (III) adsorption from dilute waste solutions onto Amberlite XAD7 resin modified with L-glutamic acid. *Sci. Rep.* 9, 8757. <https://doi.org/10.1038/s41598-019-45249-1>
- Muscolo, A., Sidari, M., Nardi, S., 2013. Humic substance: Relationship between structure and activity. Deeper information suggests univocal findings. *J. Geochem. Explor.* 129, 57–63. <https://doi.org/10.1016/j.gexplo.2012.10.012>
- Nakbanpote, W., Thiravetyan, P., Kalambaheti, C., 2002. Comparison of gold adsorption by *Chlorella vulgaris*, rice husk and activated carbon. *Miner. Eng.* 15, 549–552. [https://doi.org/10.1016/S0892-6875\(02\)00064-X](https://doi.org/10.1016/S0892-6875(02)00064-X)
- Nuryono, N., Miswanda, D., Sakti, S.C.W., Rusdiarso, B., Krisbiantoro, P.A., Utami, N., Otomo, R., Kamiya, Y., 2020. Chitosan-functionalized natural magnetic particle@silica modified with (3-chloropropyl)@trimethoxysilane as a highly stable magnetic adsorbent for gold(III) ion. *Mater. Chem. Phys.* 255, 123507.
- Parajuli, D., Inoue, K., Kuriyama, M., Funaoka, M., Makino, K., 2005. Reductive adsorption of gold(III) by crosslinked lignophenol. *Chem. Lett.* 34, 34–35. <https://doi.org/10.1246/cl.2005.34>
- Prasasti, D., Santosa, S.J., Sudiono, S., 2019. Evaluation of the adsorption and reduction of Au(III) on esterified humic acid, in: *Proceedings of the 2019 Ahmad Dahlan International*

- Conference Series on Pharmacy and Health Science (ADICS-PHS 2019).  
<https://doi.org/10.2991/adics-phs-19.2019.5>
- Rashid, M., Price, N.T., Gracia Pinilla, M.Á., O'Shea, K.E., 2017. Effective removal of phosphate from aqueous solution using humic acid coated magnetite nanoparticles. *Water Res.* 123, 353–360. <https://doi.org/10.1016/j.watres.2017.06.085>
- Rashid, M., Sterbinsky, G.E., Pinilla, M.Á.G., Cai, Y., O'Shea, K.E., 2018. Kinetic and mechanistic evaluation of inorganic arsenic species adsorption onto humic acid grafted magnetite nanoparticles. *J. Phys. Chem. C* 122, 13540–13547. <https://doi.org/10.1021/acs.jpcc.7b12438>
- Salviano, L.B., Cardoso, T.M. da S., Silva, G.C., Dantas, M.S.S., Ferreira, A. de M., 2018. Microstructural assessment of magnetite nanoparticles ( $\text{Fe}_3\text{O}_4$ ) obtained by chemical precipitation under different synthesis conditions. *Mater. Res.* 21. <https://doi.org/10.1590/1980-5373-mr-2017-0764>
- Santosa, S.J., Fitriani, D., Aprilita, N.H., Rusdiarso, B., 2020a. Gallic and salicylic acid-functionalized Mg/Al hydrotalcite as highly effective materials for reductive adsorption of  $\text{AuCl}_4^-$ . *Appl. Surf. Sci.* 507, 145115. <https://doi.org/10.1016/j.apsusc.2019.145115>
- Santosa, S.J., Krisbiantoro, P.A., Elianasari, Sutarno, 2020b. Functionalization of Mg/Al hydrotalcite and calcined Mg/Al hydrotalcite with gallic acid for reductive adsorption of tetrachloroaurate(III) ion in aqueous solution. *Int. J. Environ. Anal. Chem.* In press. <https://doi.org/https://doi.org/10.1080/03067319.2020.1807972>
- Santosa, S.J., Sudiono, S., Siswanta, D., Kunarti, E.S., Dewi, S.R., 2011. Mechanism of the removal of  $[\text{AuCl}_4]^-$  ions from aqueous solution by means of peat soil humin. *Adsorpt. Sci. Technol.* 29, 733–746. <https://doi.org/10.1260/0263-6174.29.8.733>

- Santosa, S.J., Sudiono, S., Sujandi, S., 2006. Peat soil humic acid immobilization on silica gel and its application as an adsorbent for the selective adsorption of copper. *e-J. Surf. Sci. Nanotechnol.* 4, 602–608. <https://doi.org/10.1380/ejssnt.2006.602>
- Singhal, P., Jha, S.K., Pandey, S.P., Neogy, S., 2017. Rapid extraction of uranium from sea water using  $\text{Fe}_3\text{O}_4$  and humic acid coated  $\text{Fe}_3\text{O}_4$  nanoparticles. *J. Hazard. Mater.* 335, 152–161. <https://doi.org/10.1016/j.jhazmat.2017.04.043>
- Soleimani, M., Kaghazchi, T., 2008. Adsorption of gold ions from industrial wastewater using activated carbon derived from hard shell of apricot stones – An agricultural waste. *Biores. Technol.* 99, 5374–5383. <https://doi.org/10.1016/j.biortech.2007.11.021>
- Steelink, C., Tollin, G., 1962. Stable free radicals in soil humic acid. *Biochim. Biophys. Acta* 59, 25–34. [https://doi.org/10.1016/0006-3002\(62\)90695-9](https://doi.org/10.1016/0006-3002(62)90695-9)
- Struyk, Z., Sposito, G., 2001. Redox properties of standard humic acids. *Geoderma* 102, 329–346. [https://doi.org/10.1016/S0016-7061\(01\)00040-4](https://doi.org/10.1016/S0016-7061(01)00040-4)
- Sudiono, S., Yuniarti, M., Siswanta, D., Kunarti, E.S., Triyono, T., Santosa, S.J., 2017. The role of carboxyl and hydroxyl groups of humic acid in removing  $\text{AuCl}_4^-$  from aqueous solution. *Indones. J. Chem.* 17, 95–104. <https://doi.org/10.22146/ijc.23620>
- Suyanta, S., Sudiono, S., Santosa, S.J., 2010. Determination of rate constant and stability of adsorption in competitive adsorption of Cr(III) and Cd(II) on humic acid by using the new model of kinetic formulation. *Indones. J. Chem.* 4, 161–167. <https://doi.org/10.22146/ijc.21847>

- Tuncuk, A., Stazi, V., Akcil, A., Yazici, E.Y., Deveci, H., 2012. Aqueous metal recovery techniques from e-scrap: Hydrometallurgy in recycling. *Miner. Eng.* 25, 28–37. <https://doi.org/10.1016/j.mineng.2011.09.019>
- Wright, J.B., 1964. Iron-titanium oxides in Some New Zealand ironsands. *New Zeal. J. Geol. Geop.* 7, 424–444. <https://doi.org/10.1080/00288306.1964.10422094>
- Xu, J., Yang, H., Fu, W., Du, K., Sui, Y., Chen, J., Zeng, Y., Li, M., Zou, G., 2007. Preparation and magnetic properties of magnetite nanoparticles by sol–gel method. *J. Magn. Magn. Mater.* 309, 307–311. <https://doi.org/10.1016/j.jmmm.2006.07.037>
- Yantasee, W., Warner, C.L., Sangvanich, T., Addleman, R.S., Carter, T.G., Wiacek, R.J., Fryxell, G.E., Timchalk, C., Warner, M.G., 2007. Removal of heavy metals from aqueous systems with thiol functionalized superparamagnetic nanoparticles. *Environ. Sci. Technol.* 41, 5114–5119. <https://doi.org/10.1021/es0705238>
- Yuniarti, M., 2013. Study of adsorption-reduction of  $\text{AuCl}_4^-$  on humic acid-coated magnetite ( $\text{Fe}_3\text{O}_4\text{-HA}$ ). Universitas Gadjah Mada, Yogyakarta, Indonesia.
- Zhao, G., Wang, Z., Dong, M.H., Rao, K., Luo, J., Wang, D., Zha, J., Huang, S., Xu, Y., Ma, M., 2008. PBBs, PBDEs, and PCBs levels in hair of residents around e-waste disassembly sites in Zhejiang Province, China, and their potential sources. *Sci. Total Environ.* 397, 46–57. <https://doi.org/10.1016/j.scitotenv.2008.03.010>
- Zhou, Y., Qiu, K., 2010. A new technology for recycling materials from waste printed circuit boards. *J. Hazard. Mater.* 175, 823–828. <https://doi.org/10.1016/j.jhazmat.2009.10.083>

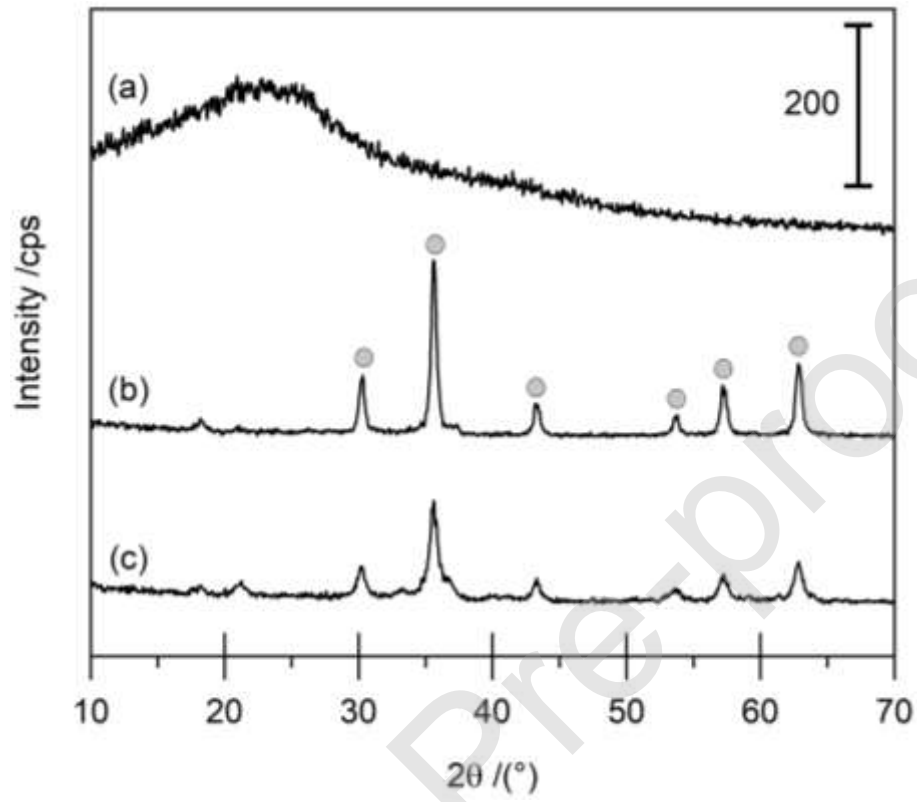


**Figure 1.** XRD patterns of (a) purified HA, (b)  $\text{Fe}_3\text{O}_4$  and (c)  $\text{Fe}_3\text{O}_4$ -HA.

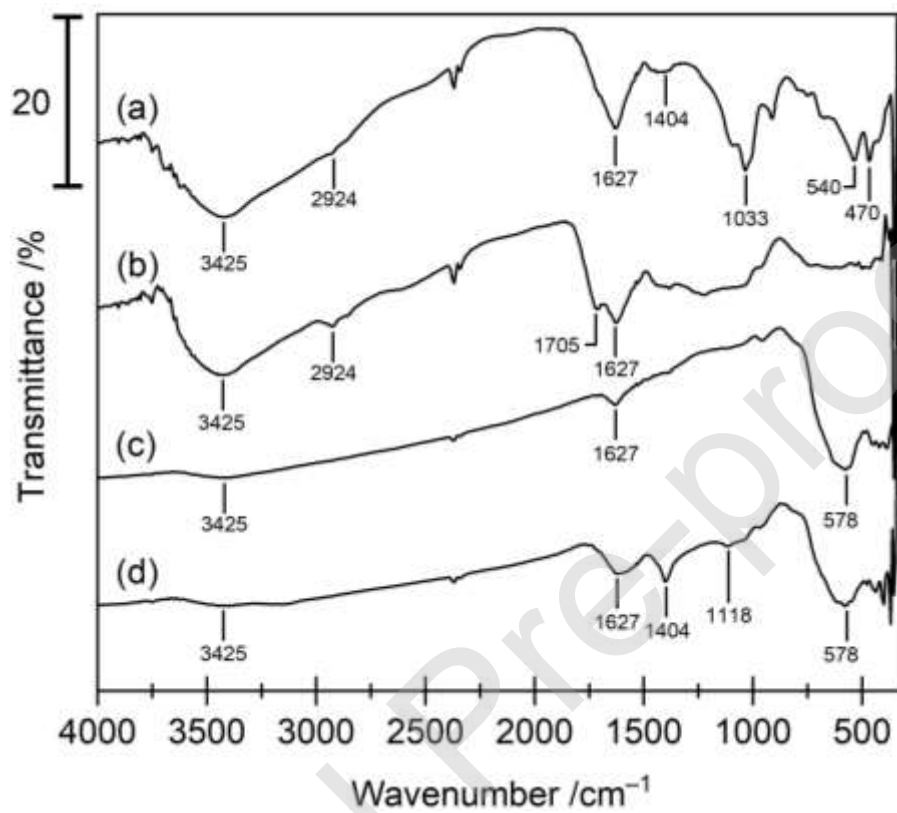


**Figure 2.** FTIR spectra of (a) crude HA, (b) purified HA, (c) Fe<sub>3</sub>O<sub>4</sub> and (d) Fe<sub>3</sub>O<sub>4</sub>-HA.

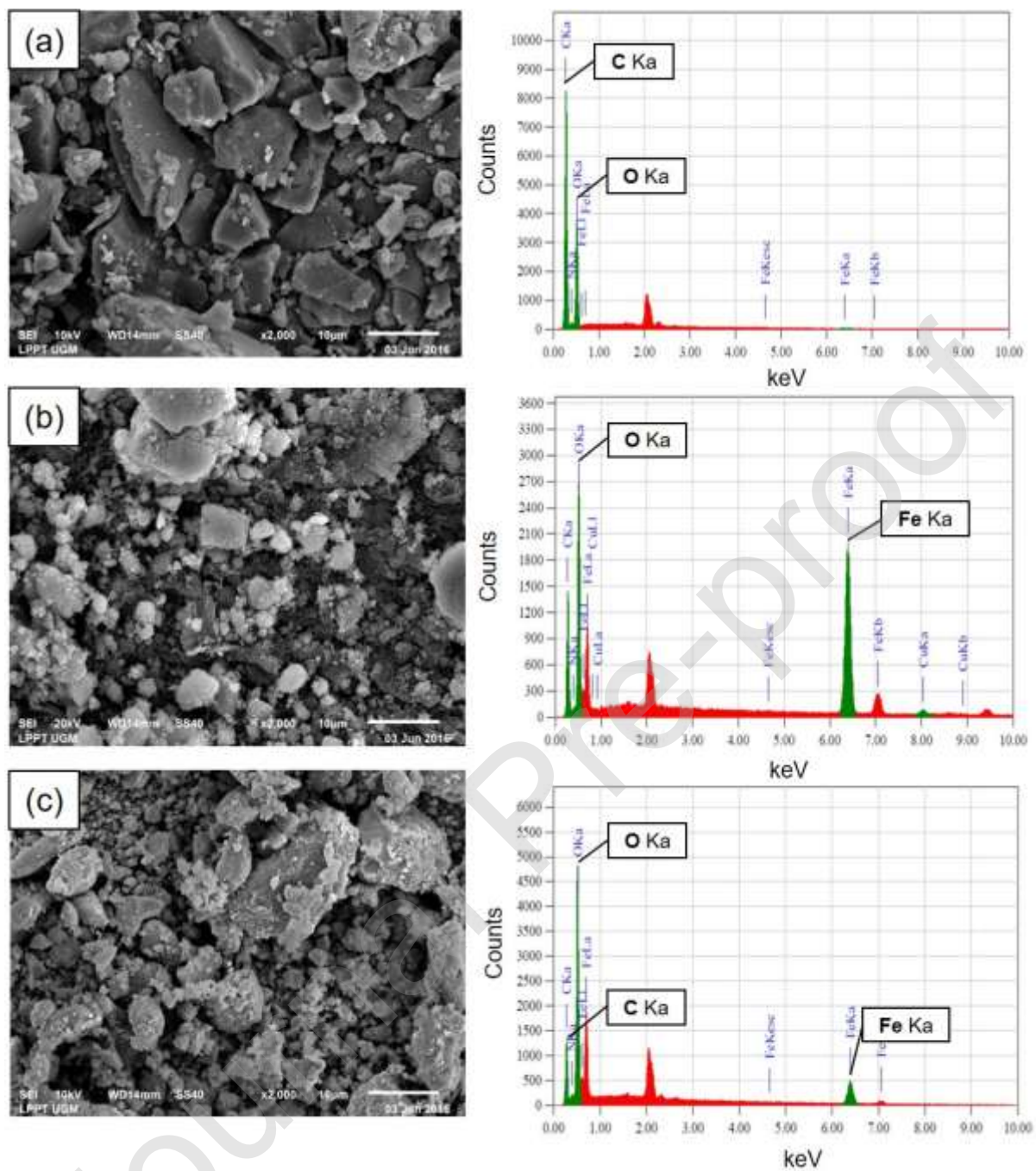


**Figure 3.** SEM images and EDS analyses of (a) HA, (b) Fe<sub>3</sub>O<sub>4</sub> and (c) Fe<sub>3</sub>O<sub>4</sub>-HA.

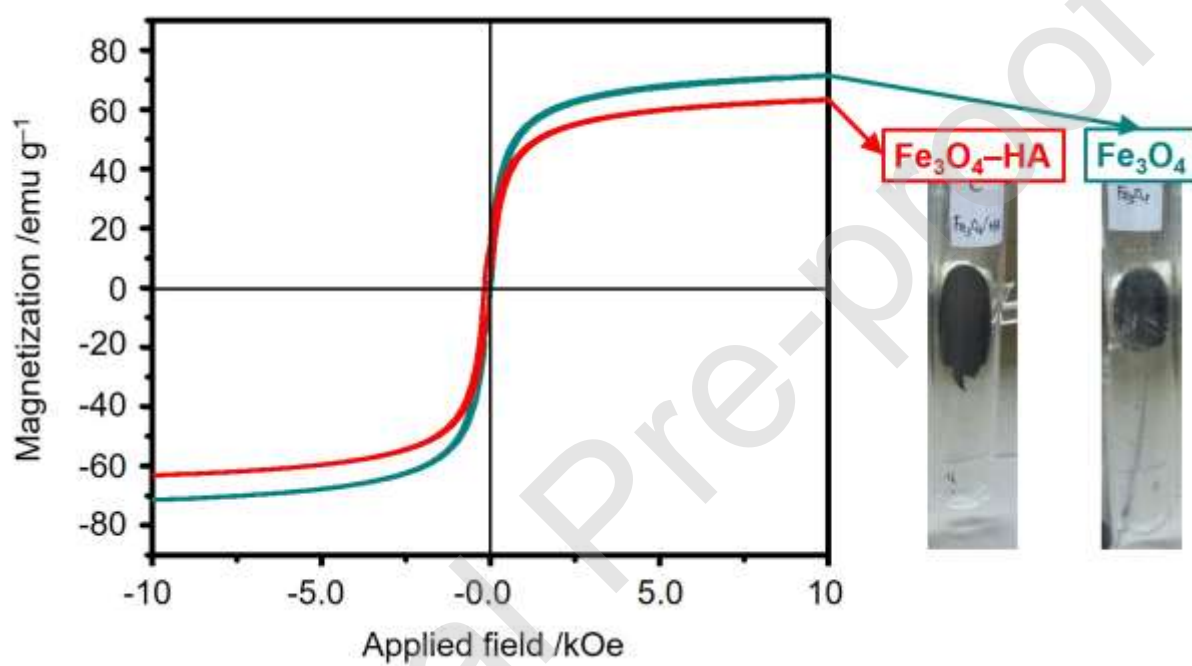


**Figure 4.** The magnetization curve and conventional magnetic test with a magnet of  $\text{Fe}_3\text{O}_4$  and  $\text{Fe}_3\text{O}_4\text{-HA}$ .

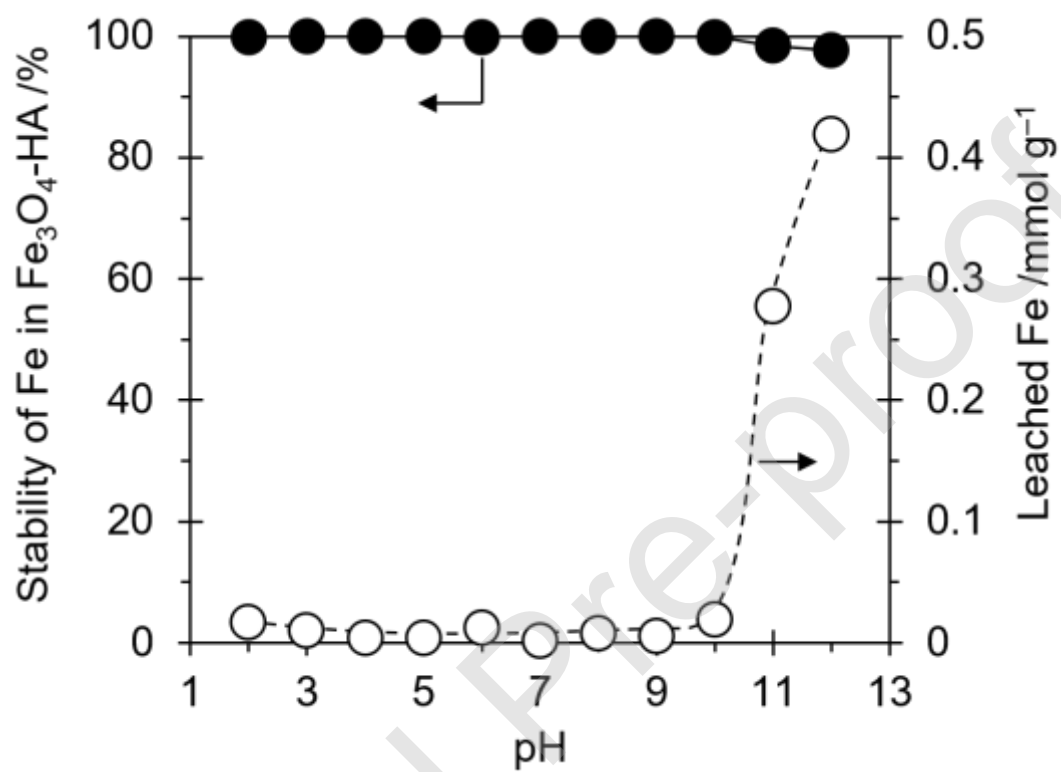


**Figure 5.** The stability of Fe in Fe<sub>3</sub>O<sub>4</sub>-HA towards dissolution.

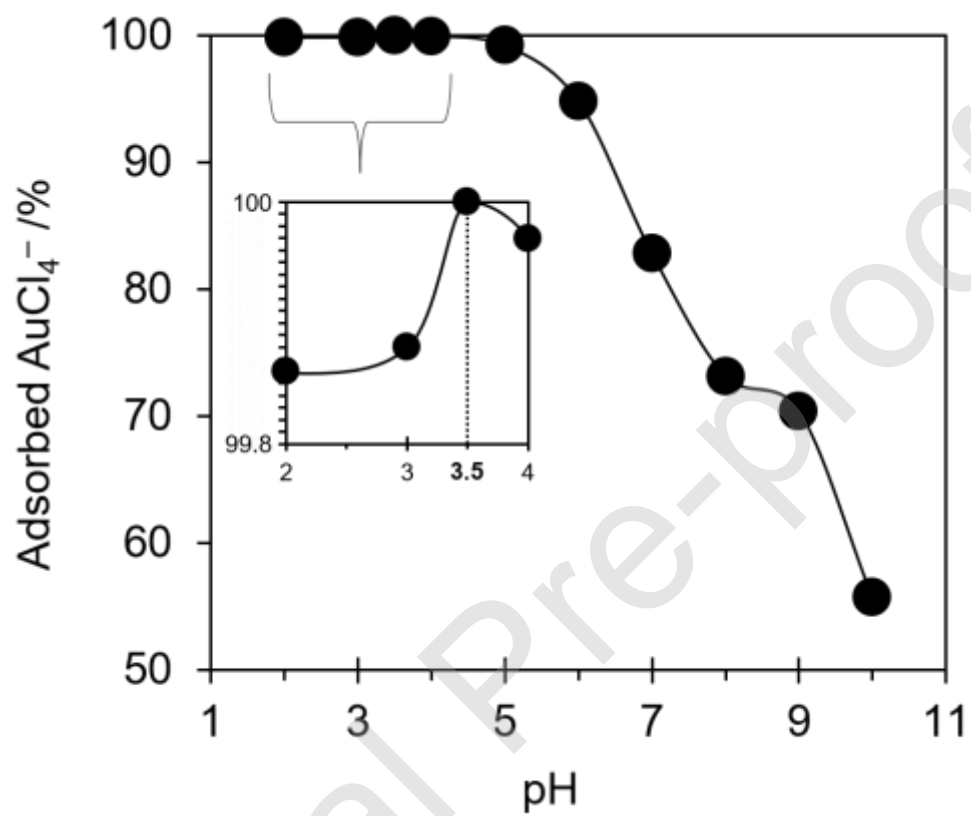


**Figure 6.** Effect of medium acidity on the percentage of adsorbed Au(III).

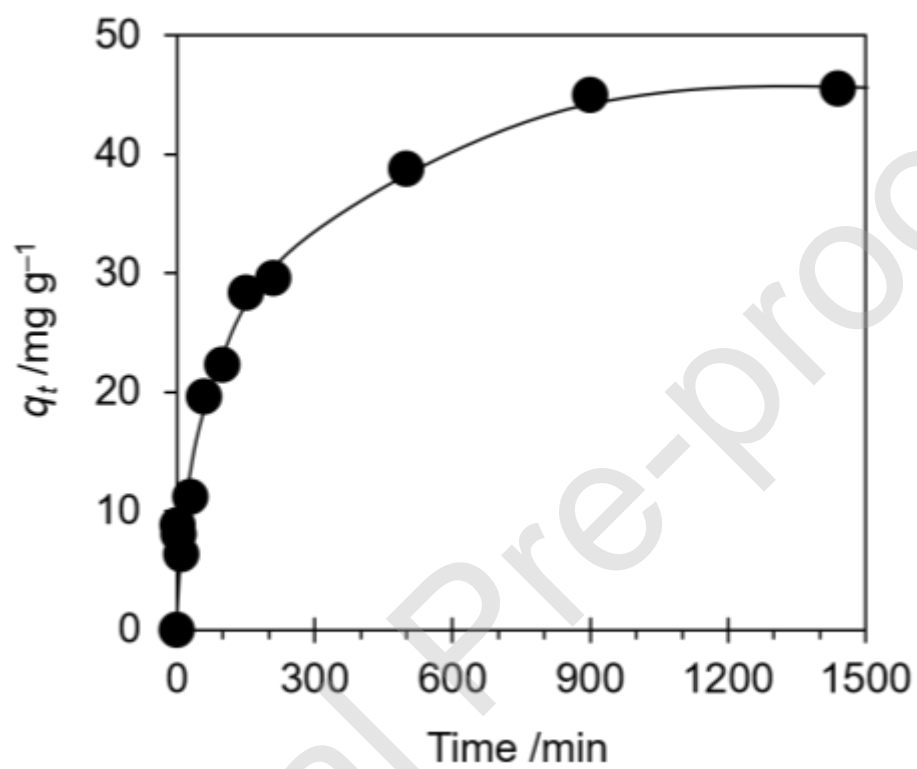


**Figure 7.** Effect of contact time on the adsorption of Au(III) on  $\text{Fe}_3\text{O}_4$ -HA.

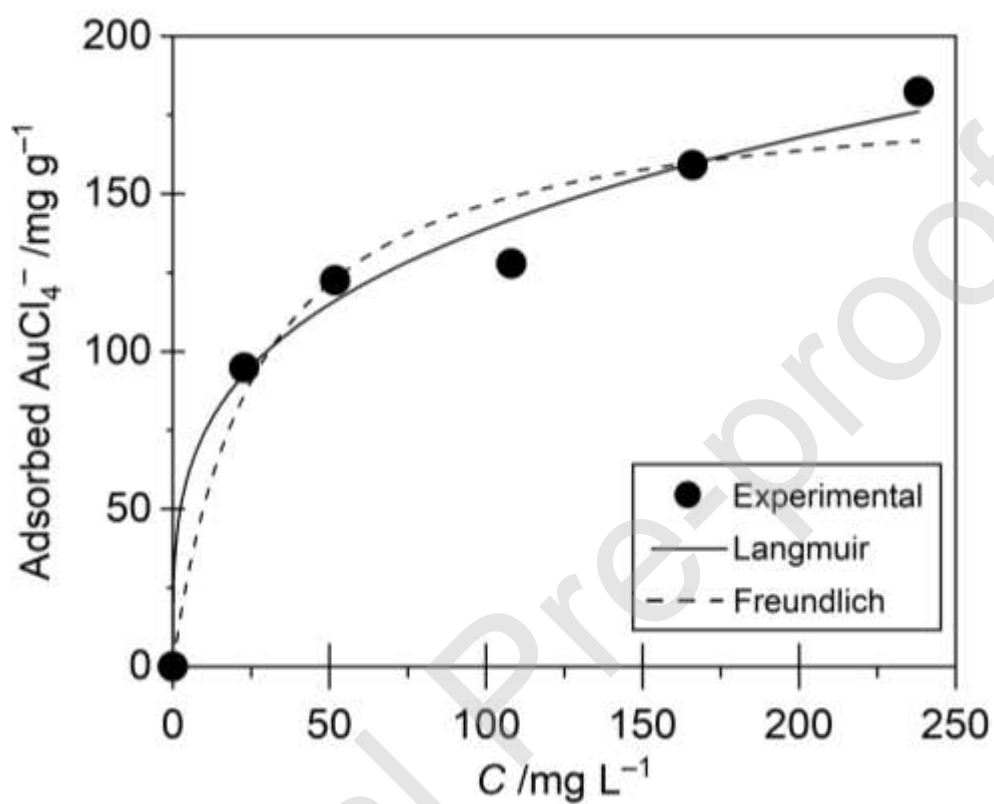


**Figure 8.** Adsorption of Au(III) on Fe<sub>3</sub>O<sub>4</sub>-HA as a function of the remaining Au(III) concentration at equilibrium ( $C$ ) as well as the adsorption profiles modelled according to the Langmuir and Freundlich isotherm models.

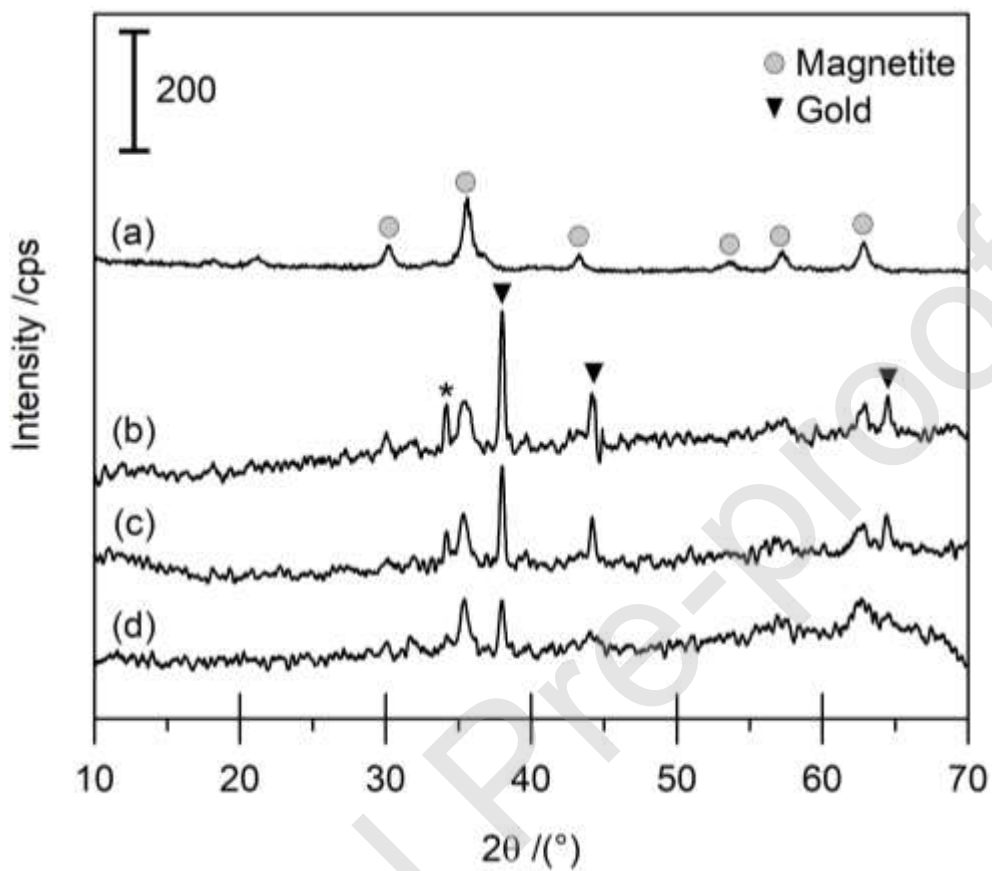


**Figure 9.** XRD spectra of Fe<sub>3</sub>O<sub>4</sub>-HA (a) before and (b) after adsorption of Au(III), and after the adsorption of Au(III) in the presence of (c) 20% and (d) 50% of 2-propanol.

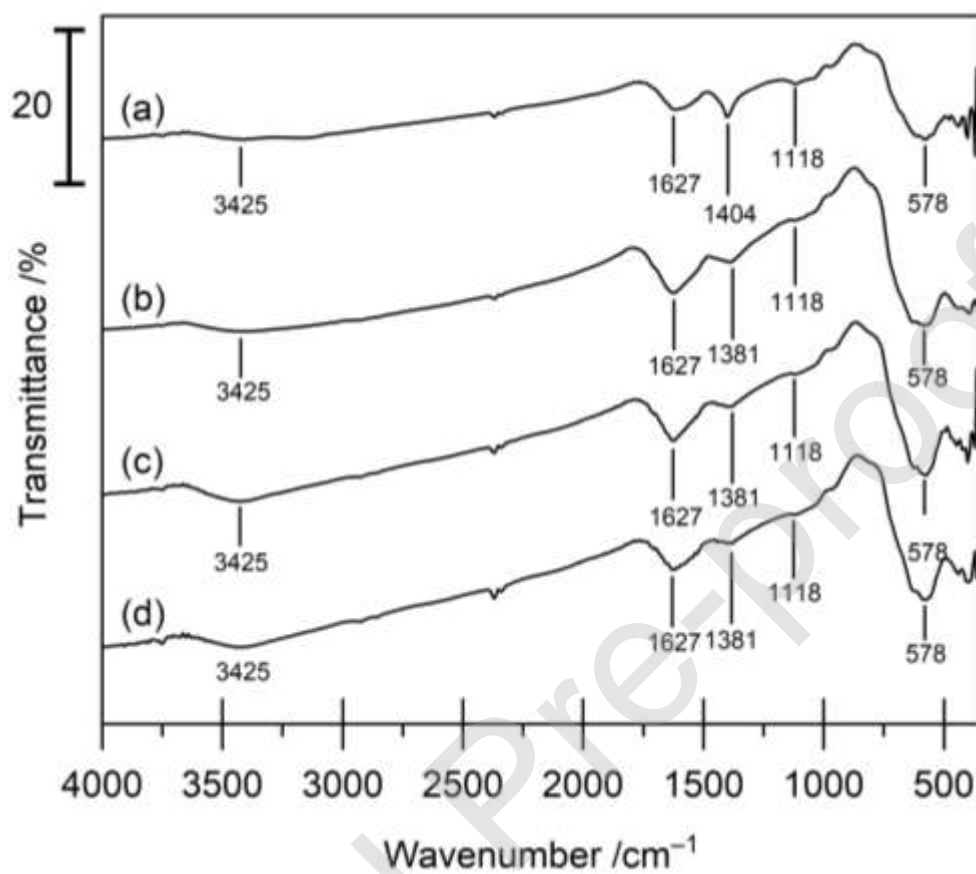


**Figure 10.** FTIR spectra of Fe<sub>3</sub>O<sub>4</sub>-HA (a) before and (b) after adsorption of Au(III), and after the adsorption of Au(III) in the presence of (c) 20% and (d) 50% of 2-propanol.

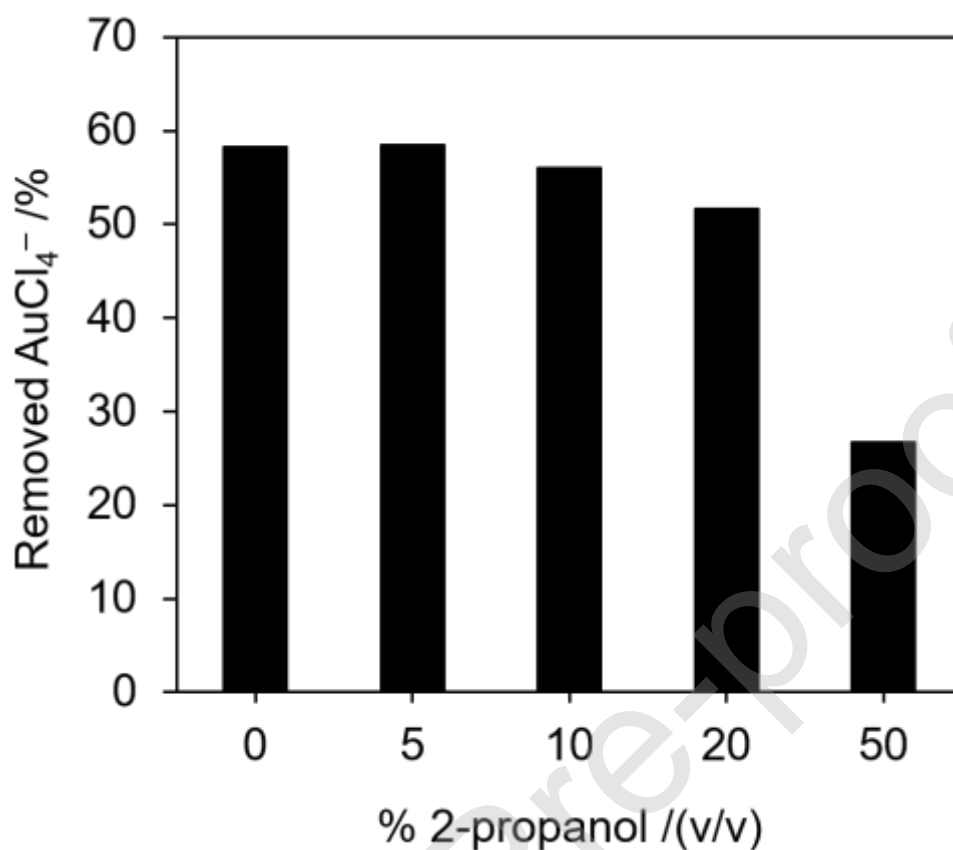


**Figure 11.** The effect of the addition of 2-propanol on the removal percentage of Au(III) from the solution. Conditions: weight of adsorbent, 5 mg; 200 mg L<sup>-1</sup> Au(III) solution, 10 mL (including 2-propanol); initial pH, 3.5; adsorption temperature, room temperature; and reaction time, 15 h.

**Table 1** EDS of HA, Fe<sub>3</sub>O<sub>4</sub> and Fe<sub>3</sub>O<sub>4</sub>-HA.

Element	HA /% wt.	Fe <sub>3</sub> O <sub>4</sub> /% wt.	Fe <sub>3</sub> O <sub>4</sub> -HA /% wt.
C	45.97	-	25.65
O	39.53	29.44	41.46
Fe	-	54.21	24.93

**Table 2** Total acidity and the content of carboxyl and phenolic hydroxyl groups of HA and Fe<sub>3</sub>O<sub>4</sub>-HA

Functional groups	Stevenson (1994) (Stevenson, 1994)/ cmol kg <sup>-1</sup>	HA / cmol kg <sup>-1</sup>	Fe <sub>3</sub> O <sub>4</sub> -HA / cmol kg <sup>-1</sup>
Total acidity	570 – 890	710.66	320.44
–COOH	150 – 570	315.79	87.43
Phenolic –OH	150 – 400	394.87	233.01

**Table 3.** First order ( $k_1$ ), first order reaching equilibrium ( $k_{1p}$ ) and pseudo-second order ( $k_{2p}$ ) rate constants for the adsorption of Au(III) by Fe<sub>3</sub>O<sub>4</sub>-HA.

First order*		First order reaching equilibrium <sup>#</sup>		Pseudo-second order <sup>@</sup>	
$R^2$	$k_1^a \times 10^{-3}$	$R^2$	$k_{1p}^b \times 10^{-3}$	$R^2$	$k_{2p}^c \times 10^{-4}$
0.9869	4.10	0.9576	3.60	0.9955	3.03

\*Santosa and Muzakky, 2002; <sup>#</sup>Langmuir-Hinshelwood; <sup>@</sup>Ho and McKay, 1999; <sup>a</sup> $k_1$  in min<sup>-1</sup>; <sup>b</sup> $k_{1p}$  in min<sup>-1</sup>; <sup>c</sup> $k_{2p}$  g mg<sup>-1</sup> min<sup>-1</sup>.

**Table 4.** Langmuir and Freundlich isotherm models for the adsorption of Au(III) by Fe<sub>3</sub>O<sub>4</sub>-HA.

Langmuir			Freundlich		
$R^2$	$K^a$	$b^b \times 10^{-4}$	$R^2$	$1/n$	$B^c \times 10^{-3}$
0.9854	0.1389	200	0.9359	0.132	75.33

<sup>a</sup> $K$  in L mg<sup>-1</sup>; <sup>b</sup> $b$  in mg g<sup>-1</sup>; <sup>c</sup> $B$  in mg g<sup>-1</sup>.

**Table 5** Adsorption capacities of some reported adsorbents for the removal of Au(III).

Adsorbent	Adsorption capacity /mg g <sup>-1</sup>	Ref.
Fe <sub>3</sub> O <sub>4</sub> -HA	200	This work
Activated Carbon	1.254	(Soleimani and Kaghazchi, 2008)

Chitosan-Fe <sub>3</sub> O <sub>4</sub> @SiO <sub>2</sub> -(3-chloropropyl)trimethoxysilane	112	(Nuryono et al., 2020)
HA	192	(Prasasti et al., 2019)
Esterified HA	625	(Prasasti et al., 2019)
Fe <sub>3</sub> O <sub>4</sub> -fulvic acid	44.85	(Krisbiantoro et al., 2017)
Mg/Al hydrotalcite-gallic acid	175.43	(Santosa et al., 2020b)
L-lysine modified crosslinked chitosan resin	70.34	(Fujiwara et al., 2007)
Rice husk ash	50.50	(Nakbanpote et al., 2002)

---